



## OPEN ACCESS

## EDITED BY:

Guangzhe Jin,  
Guangdong Ocean University, China

## REVIEWED BY:

Xu Dong,  
Ministry of Natural Resources, China  
Shiguo Wu,  
Institute of Deep-Sea Science and  
Engineering (CAS), China

## \*CORRESPONDENCE:

Zhenyu Lei  
44231234@qq.com  
Ming Su  
suming3@mail.sysu.edu.cn

## SPECIALTY SECTION:

This article was submitted to  
Marine Biogeochemistry,  
a section of the journal  
Frontiers in Marine Science

RECEIVED: 17 May 2022

ACCEPTED: 24 June 2022

PUBLISHED: 22 July 2022

## CITATION:

Liu S, Liang Z, Zhang B, Su H, Lei Z  
and Su M (2022) Carbonate contourite  
drifts in the southwest South China  
Sea: Sedimentary, paleoceanographic  
and economic implications.  
*Front. Mar. Sci.* 9:946231.  
10.3389/fmars.2022.946231

## Copyright

© 2022 Liu, Liang, Zhang, Su, Lei  
and Su. This is an open-access  
article distributed under the terms of  
the [Creative Commons Attribution  
License \(CC BY\)](https://creativecommons.org/licenses/by/4.0/). The use, distribution  
or reproduction in other forums  
is permitted, provided the original  
author(s) and the copyright owner(s)  
are credited and that the original  
publication in this journal is cited, in  
accordance with accepted academic  
practice. No use, distribution or  
reproduction is permitted which does  
not comply with these terms.

# Carbonate contourite drifts in the southwest South China Sea: Sedimentary, paleoceanographic and economic implications

Shan Liu<sup>1,2</sup>, Zijun Liang<sup>1</sup>, Boda Zhang<sup>1</sup>, Haixia Su<sup>1</sup>, Zhenyu Lei<sup>3\*</sup> and Ming Su<sup>1,2,4\*</sup>

<sup>1</sup>School of Marine Science, Sun Yat-sen University, Zhuhai, China, <sup>2</sup>Southern Marine Science and Engineering Guangdong Laboratory (Zhuhai), Zhuhai, China, <sup>3</sup>Guangzhou Marine Geology Survey, China Geological Survey, Ministry of Natural Resources, Guangzhou, China, <sup>4</sup>Guangdong Provincial Key Laboratory of Marine Resources and Coastal Engineering, Guangzhou, China

Contourite drifts are significant sedimentary features and provide clues for the reconstruction of paleoceanography and paleoenvironment. Although they have been increasingly identified in the world's ocean, shallow-water contourite drifts (< 300 m depth) remain poorly understood and the examples are rare. This study documents a Middle Miocene shallow-water contourite depositional system in the southwest South China Sea by interpreting seismic reflection data and calibrating results with the previous chronological framework. The depositional system consisted of six mounded drifts and six moats. The contourite features were generated in seismic unit III (16–10.5 Ma) and distributed adjacent to carbonate reefs. They were formed on the proto-continental shelf (50–200 m depth) and shaped by the wind-driven currents. Changes in the sedimentary stacking patterns suggest three evolutionary stages of the contourite features. Stage I represents the growth of the Middle Miocene contourite depositional system between 16 and 10.5 Ma. Stage II marks the termination of carbonate drifts and the burial of the Late Miocene sedimentation during 10.5–5.3 Ma. Stage III started with the development of modern deep-water sedimentary systems since 5.3 Ma. The contourite features are compared with the examples on other South China Sea margins. Significant changes in the paleoceanography occurred at 10.5 Ma and 6.5–5.3 Ma when the dominated bottom currents shifted from the monsoonal wind-driven currents to the North Pacific waters, and then the modern circulation system. The Middle Miocene mounded drifts were likely sourced by the coarse-grained carbonate sands. Fluid flow escaped from the coarse-grained contourite layers and natural gas leakage occurs on the seafloor. Shallow-water carbonate contourite drifts can be served as a good gas reservoir and have great economic potential.

## KEYWORDS

contourite depositional system, sedimentary process, bottom current, carbonate reef, southwest South China Sea

# 1 Introduction

Bottom currents are vital oceanographic processes of redistributing sediments (Hanebuth et al., 2015; de Castro et al., 2021; Rodrigues et al., 2022), shaping seafloor morphology (Howe et al., 2006; Hernández-Molina et al., 2017; Yin et al., 2022), influencing marine ecosystems (Loeb et al., 2010; Cimino et al., 2020), and transporting pollutants (Martin et al., 2017; Kane and Clare, 2019). The persistent bottom currents that are commonly driven by winds, thermohaline circulation, eddies, and tides can create alongslope sedimentary features on the continental margin through geological timescales (Hernández-Molina et al., 2008; Rebesco et al., 2014). The combination of the depositional (i.e., contourite drifts) and erosional features (i.e., moats, contourite channels), known as the contourite depositional system, provides clues for the reconstruction of palaeoceanographic and paleoenvironmental conditions (Llave et al., 2007; García et al., 2016; de Weger et al., 2020; Kirby et al., 2021).

Since the 1960s (Heezen and Hollister, 1964; Heezen et al., 1966), contourite depositional systems have been increasingly observed in the deep basins (García et al., 2016; Pérez et al., 2019; Ng et al., 2021), on the continental slopes (Roque et al., 2012; Hernández-Molina et al., 2016; Yin et al., 2019), in the shallow marine (Pepe et al., 2018; Mulder et al., 2019), and in lakes (Ceramicola et al., 2001; Wagner et al., 2012). However, identified shallow-water contourite drifts are not as much as deep-water ones (Thran et al., 2018). Shallow-water contourite drifts are those influenced by contour-parallel flows at a water depth shallower than 300 m (Verdicchio and Trincardi, 2008). Some of the well-studied examples are the Maldives (Lüdmann et al., 2013; Betzler et al., 2018) and the Bahamas (Chabaud et al., 2016; Mulder et al., 2019) archipelagos. The contourite depositional systems were formed adjacent to carbonate reefs, platforms, or atolls and situated in the pathway of major surface currents (Lüdmann et al., 2013; Betzler et al., 2014). This type of drifts, defined as carbonate contourite drifts, commonly consisted of coarse-grained carbonated sediments and has an economic significance for hydrocarbon exploration (Viana, 2008; Eberli and Betzler, 2019).

In the tropical Pacific Ocean, the Middle Miocene was an important period for the shallow-water carbonate drifts because of widely distributed carbonate platforms and enhanced surface currents (Lüdmann et al., 2013; Betzler et al., 2018; Mathew et al., 2020). The proto-continental shelf in the South China Sea was under the comparable paleoceanographic and paleoenvironmental conditions and served as a preferable region for the development of carbonates during the Middle Miocene (Wu et al., 2016; Yan et al., 2020; Makhankova et al., 2021; Yang et al., 2021). The formation of the carbonate contourite drifts would be theoretically significant as the case of the Maldives (Lüdmann et al., 2013; Betzler et al., 2014). However, studies on the shallow-water carbonate drifts in the South China Sea are rare.

The sedimentary, paleoceanographic, and economic implications of the carbonate contourite drifts remain poorly investigated.

This study focuses on the continental margin in the southwest South China Sea, which offers a key area to study carbonate contourite drifts and contributes to a better understanding of South China Sea paleoceanography. The objectives of this work are: 1) to identify the Middle Miocene contourite depositional system; 2) to determine the contourite evolutionary stages; 3) to discuss paleoceanographic changes in the South China Sea; and 4) to demonstrate the economic importance of shallow-water carbonate drifts.

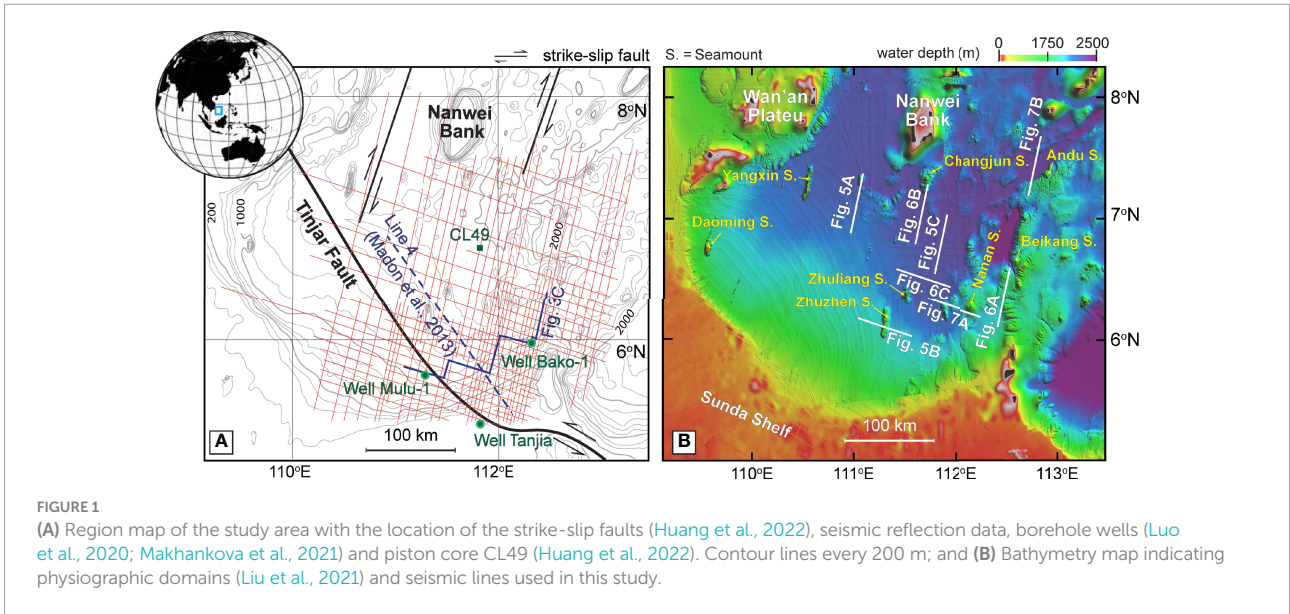
## 2 Regional setting

### 2.1 Geological setting

The South China Sea is a marginal sea located in the NW Pacific Ocean. Seafloor spreading and tectonic opening of the South China Sea initiated during the Cenozoic at ~33–30 Ma (Sibuet et al., 2016). In the southwest South China Sea, sedimentary basins were subsequently formed and further separated by the NW-SE orientated Tinjar fault (Figure 1A) (Morley, 2002; Barckhausen and Roeser, 2004). The basins were widened because of the widespread extensional tectonics during the Middle and Late Eocene (Hall, 2002; Hutchison, 2004). The direction of the seafloor spreading significantly changed during the Early Miocene in the South China Sea (~23–16 Ma) (Chang et al., 2022). Regional collision consequently uplifted the sedimentary basins (Hutchison, 2004; Cullen, 2010). The southwest South China Sea went into a regional quiescence stage and rapid subsidence occurred from the Middle Miocene (~10.5 Ma) onward (Hutchison, 2004; Madon et al., 2013; Zhang et al., 2020).

### 2.2 Physiographic domains

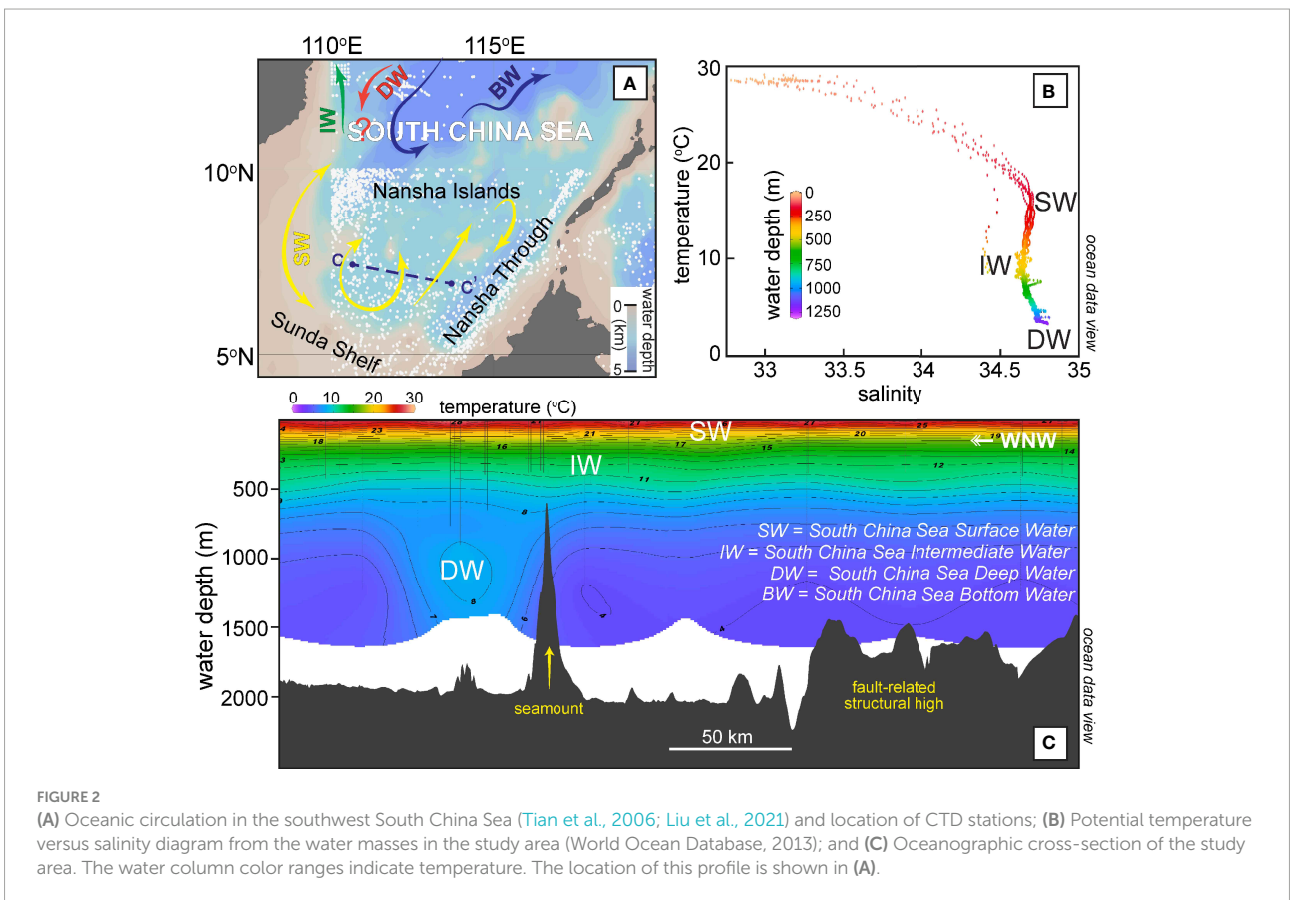
The southwest South China Sea consists of several physiographic domains (Liu et al., 2021). The Sunda continental shelf extends from 0 to 260 m water depth (Figure 1B). Modern carbonate reefs are widely observed on the shelf (Mathew et al., 2020). The continental slope extends to the Nanwei Bank (also known as the Rifleman Bank) and the Wan'an Plateau from 260 to 2360 m water depth (Figure 1B). Eight seamounts are shown. They are the Daoming, Yangxin, Zhuzhen, Zhuliang, Changjun, Nanan, Beikang, and Andu seamounts from the west to the east, respectively (Figure 1B). Modern sedimentary systems on the continental slope contain mass-transport deposits (MTDs), contourite drifts, turbidites, and pockmarks (He et al., 2018; Zhang et al., 2020; Liu et al., 2021; Huang et al., 2022).



### 2.3 Present-day oceanography

The modern oceanic circulation in the South China Sea consists of the Surface (SW), Intermediate (IW), Deep (DW), and Bottom (BW) waters from the surface to the sea bottom (Tian et al., 2006). The SW that appears from 0 and 300 m water depth

has a seasonal variation and is under the influence of monsoon winds (Figure 2A) (Qu et al., 2009). The IW is sourced from the North Pacific Intermediate Water (NPIW) (Tian et al., 2006). The water mass circulates in an anticyclonic pattern and entered the southern SCS between a water depth of 300 and 750 m (Figures 2B, C). The DW that originated from the North Pacific



Deep Water (NPDW) is observed below a water depth of 1500 m around the Luzon Strait (Qu et al., 2006). The DW is characterized by a cyclonic circulation pattern and the core is 200-300 m shallower in the southern South China Sea (Figure 2C) (Liu et al., 2021). The BW is a deep-water overflow transported through the Luzon Strait into the SCS (Zhou et al., 2017). It moves below a water depth of 2000 m in a cyclonic flowing pattern (Figure 1) (Tian et al., 2006).

### 3 Data and methods

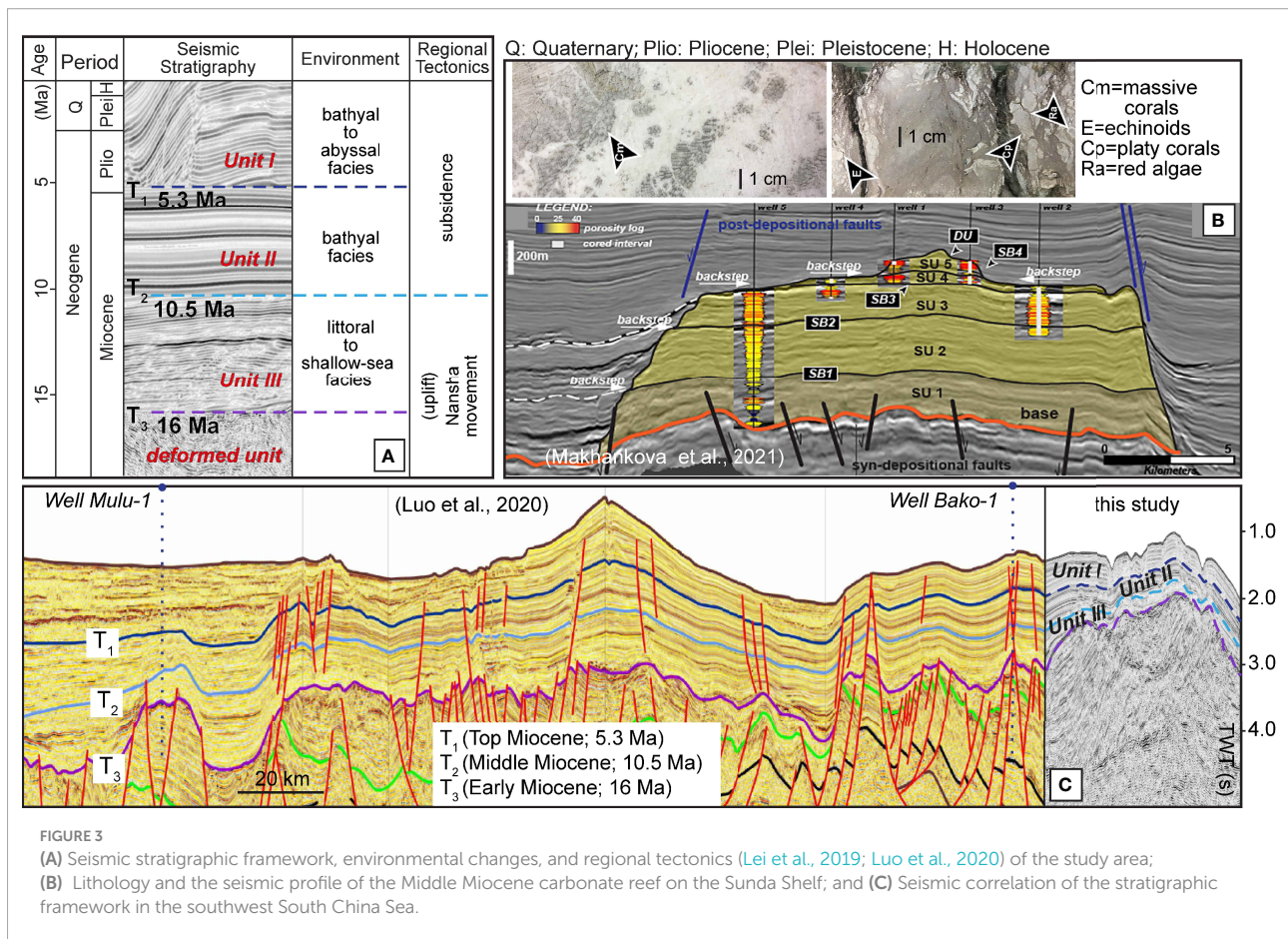
#### 3.1 Bathymetry, seismic, and oceanographic data

The datasets used for this study contain high-resolution multibeam bathymetry, multichannel seismic reflection profiles, and oceanographic observation (Figures 1, 2). Bathymetric and seismic datasets were obtained during the R/V Tanbao cruise in 1996, 2009, and 2013 via the Guangzhou Marine Geological Survey. A SeaBEAM 2112 system was used for acquiring multibeam bathymetry. The system operated at a center frequency of 12 kHz with a swath width of 120 degrees. The multichannel

seismic data were acquired by using a Seal 408 streamer recording system. The seismic source was a 32-bolt airgun array with a total volume of 5080 in<sup>3</sup>. The dominant frequency ranged from 40 to 60 Hz. The seismic reflection data were further processed by applying a bandpass filter, amplitude recovery, velocity analysis, and pre-stack time migration. Vertical CTD profiles were extracted from the World Ocean Database (2013) (Figure 2) (Boyer et al., 2013). The temperature cross-section (Figure 2C) was made utilizing the Ocean Data View (ODV) software.

#### 3.2 Seismic interpretation methods

The seismic reflection profiles are interpreted using the Petrel software. The vertical scale is expressed by two-way travel time (TWT). The seismic stratigraphic division for major depositional units is based on the identification of regional discontinuities (T<sub>3</sub>, T<sub>2</sub>, and T<sub>1</sub>) (Catuneanu et al., 2009). T<sub>3</sub> is marked as a regional erosional discontinuity, while T<sub>2</sub> and T<sub>1</sub> are identified by the vertical variation of acoustic facies (Figure 3A). These discontinuities are matched with the seismic stratigraphic documented by Luo et al. (2020) through connected seismic profiles (Figure 3C). The correlation between seismic data and drill core data (Well Mulu-1



and Bako-1) indicate possible chronostratigraphic constraint of the study area (Figure 3).

The interpretation of contourite drifts is based on the mounded geometry, continuous oblique to subparallel reflections, and onlap reflection terminations, while moats are characterized by U-shaped erosional features (Faugères et al., 1999; Faugères and Stow, 2008; Rebesco et al., 2014). Carbonate reefs are characterized by the mounded geometry, disrupted to chaotic reflections, and bi-directional downlap reflection terminations (Figure 4) (Burgess et al., 2013; Hendry et al., 2021).

## 4 Results and interpretation

### 4.1 Seismic stratigraphic analysis

Three major seismic units (UIII–UI from old to young), separated by main discontinuities ( $T_3$ ,  $T_2$ , and  $T_1$ ), are identified below the present seafloor in the seismic profiles (Figure 3A). UIII is characterized by moderate to high amplitude and semi-continuous chaotic-subparallel reflections. The unit is separated from the base unit by discontinuity  $T_3$  (Figure 5). Mounded features with onlap and downlap terminations are identified on the continental slope and at the seamount flanks (Figures 5, 6). Some mounded features are only observed at the lower part of UIII (Figures 5C, 6C). The unit has a maximum sedimentary thickness of 1 s TWT at the lower continental shelf, but the thickness decreases seawards (Figure 3C).

UII is bounded by discontinuity  $T_2$  at its base. The unit consists of high amplitude and continuous subparallel reflections (Figures 5, 6). The sedimentary thickness is relatively constant at about 0.2 s TWT. UI is bounded by discontinuity  $T_1$  at the base and by the seafloor at its top. The unit is internally characterized by moderate-high amplitude and continuous oblique-subparallel reflections. Several fault-controlled contourite drifts were previously identified in the upper part of this unit (Figure 10)

(Liu et al., 2021). The thickness of this unit reaches the maximum value (1.2 s TWT) at the depositional section of MTDs (Figure 10) (He et al., 2018).

### 4.2 Buried carbonate reefs

Mounded features were widely observed atop discontinuity  $T_3$  in the study area (Wu et al., 2016; Yan et al., 2020). Their internal seismic features are moderate to high amplitude and disrupted to chaotic reflections, while the external shape is characterized by the mounded geometry (Figure 6). The boundary of these mounded features exhibits high amplitude reflectors. Bi-directional downlap terminations are shown (Figure 4). Although volcanism was active during the early Miocene in the study area (Yan et al., 2008), these features are not likely the volcanogenic mounds. Volcanogenic mounds are generally characterized by pull-up features and volcanic intrusion (or direct connection with sills) in seismic profiles (Magee et al., 2013), which do not match with the observation in the study area (Figures 5, 6). Besides, evidence from drilling demonstrates that these mounded features possibly contained skeletal grainstone and coral framestone with massive corals (Figure 3B) (Makhankova et al., 2021). Drillings from the adjacent regions, such as the Dangerous Ground, also show the presence of mounded carbonate reefs (Steuer et al., 2014; Banerjee and Ahmed Salim, 2021; Li et al., 2022). Thus, these mounded features are most likely the carbonate reefs.

Buried carbonate reefs were previously observed on the Sunda Shelf (Mathew et al., 2020) and the continental slope (Yan et al., 2020) (Figures 3B, 7). In addition to these identified ones, three carbonate reefs (A, B, and C) are recognized in UIII in this study (Figure 7). U-shaped erosional features and mounded depositional features are observed on one side of the carbonate reefs A, B, and C (Figure 6). Carbonate reef A was 0.7 s TWT high, and the width reached 8 km. Carbonate reef B was 0.6 s TWT high and 7 km wide. The height and width of carbonate reef

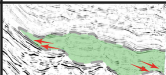
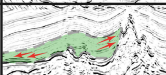
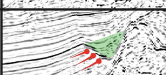
feature	example	termination	amplitude	reflection	shape	distribution	unit
mounded drifts 1-3		onlap downlap	low to moderate	oblique to subparallel	mounded	seamount, structural high	UIII
mounded drifts 4-6		onlap downlap	moderate	oblique to subparallel	mounded	carbonate reef	UIII
moat		truncation	—	—	U-shaped	mounded drift	UIII
carbonate reef		bi-directional downlap	moderate to high	disrupted to chaotic	convex to mounded	widely distributed	UIII

FIGURE 4  
Seismic expression, distribution, geometry, and examples of contourite features and carbonate reefs in seismic unit III.

C were 0.3 s TWT and 6 km. The top of carbonate reefs A and B reached  $T_2$ , while carbonate reef C only grew to the middle part of UIII (Figure 6).

## 4.3 A buried contourite depositional system

### 4.3.1 Mounded drifts

Six mounded drifts (MD 1-6) are identified in UIII (Figs. 5 and 6). MD-3 and -6 only show at the lower part of UIII (Figs. 5C and 6C). MD -1, -2, and -3 are characterized by moderated amplitude and oblique to subparallel reflections (Figure 4). Low-angle onlap and downlap terminations are observed onto  $T_3$  (Figures 4, 5). MD-1 was 0.4 s TWT thick and 21 km wide and extended along a structural high between 2.8 and 3.4 s TWT (Figure 5A). MD-2 was distributed along the southern flank of the Zhuzhen Seamount between 2.9 and 4.0 s TWT (Figures 5B, 7). The thickness was 0.3 s TWT and the width reached 17 km. MD-3 was relatively thin and only generated at the lower part of UIII between 3.3 and 4.2 s TWT (Figure 5C). The drift was 0.15 s TWT thick and 16 km wide.

MD -4, -5, and -6 are associated with carbonate reefs A, B, and C in UIII, respectively (Figure 6). These drifts exhibit moderate amplitude and oblique to subparallel reflections (Figure 6). High-angle onlap terminations are recognized onto carbonate reefs, while low-angle downlap terminations are shown towards  $T_3$  (Figs. 4 and 6). MD-4 was 0.4 s TWT thick and 9 km wide. The drift extended along the southern flank of carbonate reef A between 2.1 and 2.7 s TWT (Figs. 6A and 8). MD-5 was distributed along the southern flank of carbonate reef B between 2.6 and 3.6 s TWT (Figs. 6B and 8). The thickness was 0.4 s TWT and the width reached 11 km. MD-6 was located along the western flank of carbonate reef C between 2.5 and 2.9 s TWT (Figs. 6C and 8). The drift was generated at the lower part of UIII with a thickness of 0.3 TWT and a width of 11 km.

### 4.3.2 Moats

Six moats (Mo 1-6) were associated with the mounded drifts in UIII (Figs. 5, 6, and 8). The distribution was parallel to the seamount, structural high, and carbonate reefs (Figure 7). They were W-E and NNE-SSW orientated and exhibited truncations and U-shaped geometry (Figure 4). The incision was around 50 ms TWT and the width ranged from 0.7 to 4 km (Figures 5, 6).

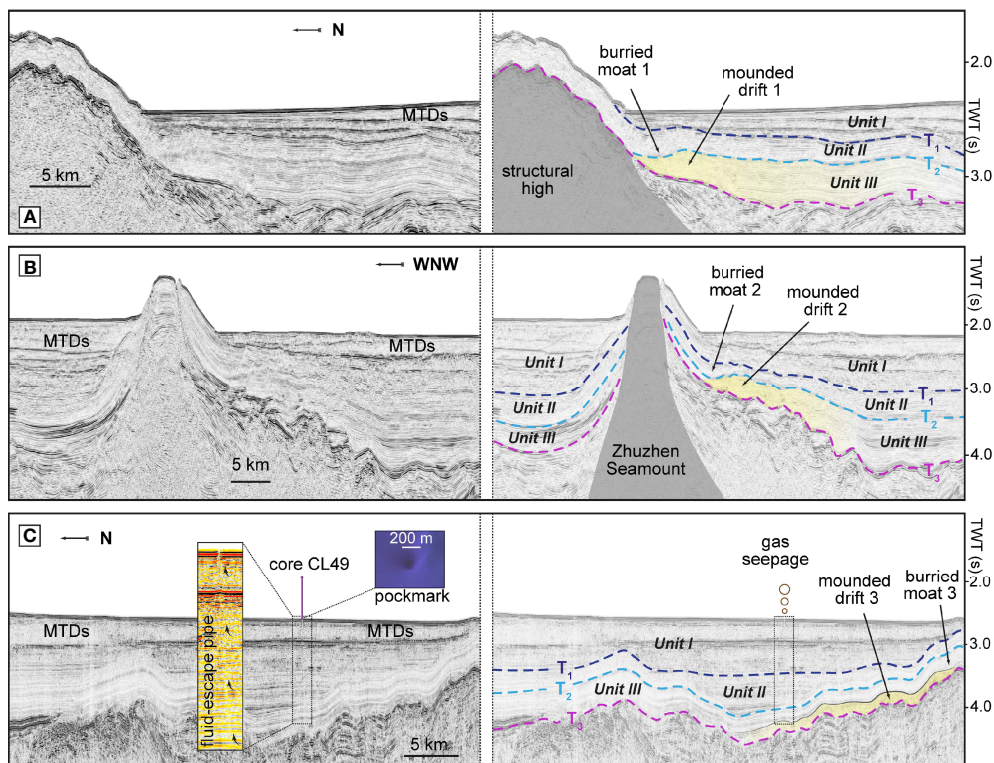


FIGURE 5

Seismic profiles and their interpretation, showing mounded drifts 1-3 and associated moats in seismic unit III. The location of these seismic lines is displayed in Figure 1B. Discontinuities  $T_3$  (16 Ma; purple dotted line),  $T_2$  (10.5 Ma; light blue dotted line) and  $T_1$  (5.3 Ma; dark blue dotted line) are indicated. A fluid-escape pipe and its expression at the seafloor are shown in (C).

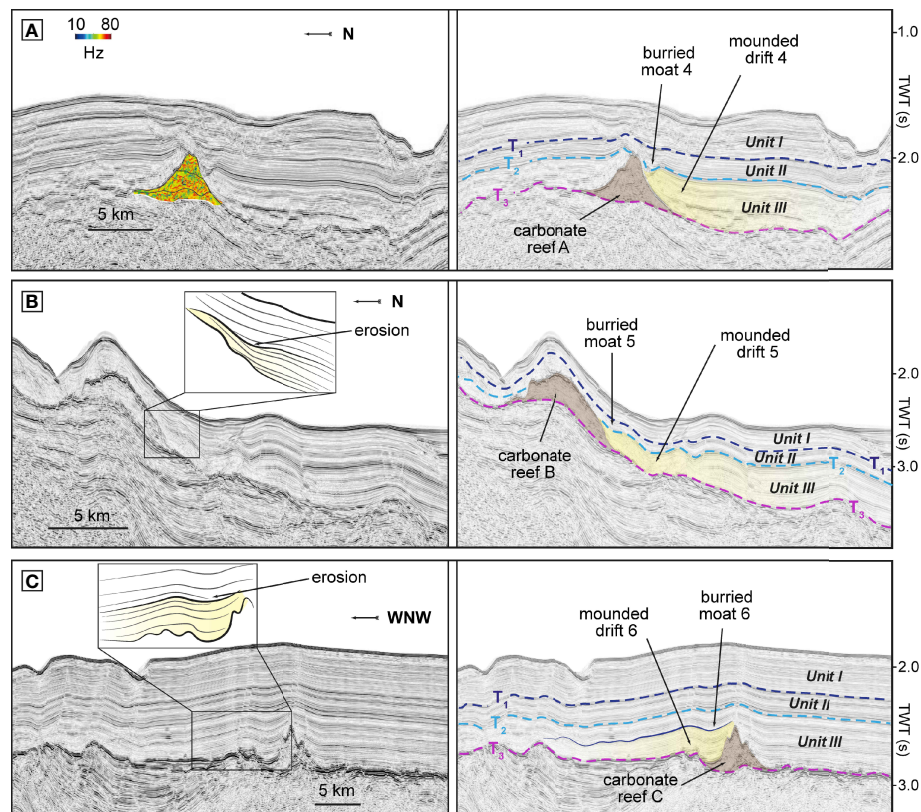


FIGURE 6

Seismic profiles and their interpretation, showing carbonate mounded drifts 1-3, associated moats, and carbonate reefs (A-C) in seismic unit III. The location of these seismic lines is displayed in Figure 1B. Discontinuities  $T_3$  (16 Ma; purple dotted line),  $T_2$  (10.5 Ma; light blue dotted line), and  $T_1$  (5.3 Ma; dark blue dotted line) are indicated. Instantaneous frequency profile of carbonate reef A is indicated in (A).

#### 4.4 A fluid-escape pipe

A fluid-escape pipe, previously identified by Huang et al. (2022), extends from UIII to the seafloor. The root of the pipe is located at the lower part of MD-3 (Figure 5C). This fluid-escape pipe shows pulled-up reflections. The seafloor expression of the pipe is a pockmark with a diameter of 210 m (Figure 5C). A piston core CL49 acquired at this location indicated the formation of gas seepage conduits at the seafloor (Huang et al., 2022).

### 5 Discussion

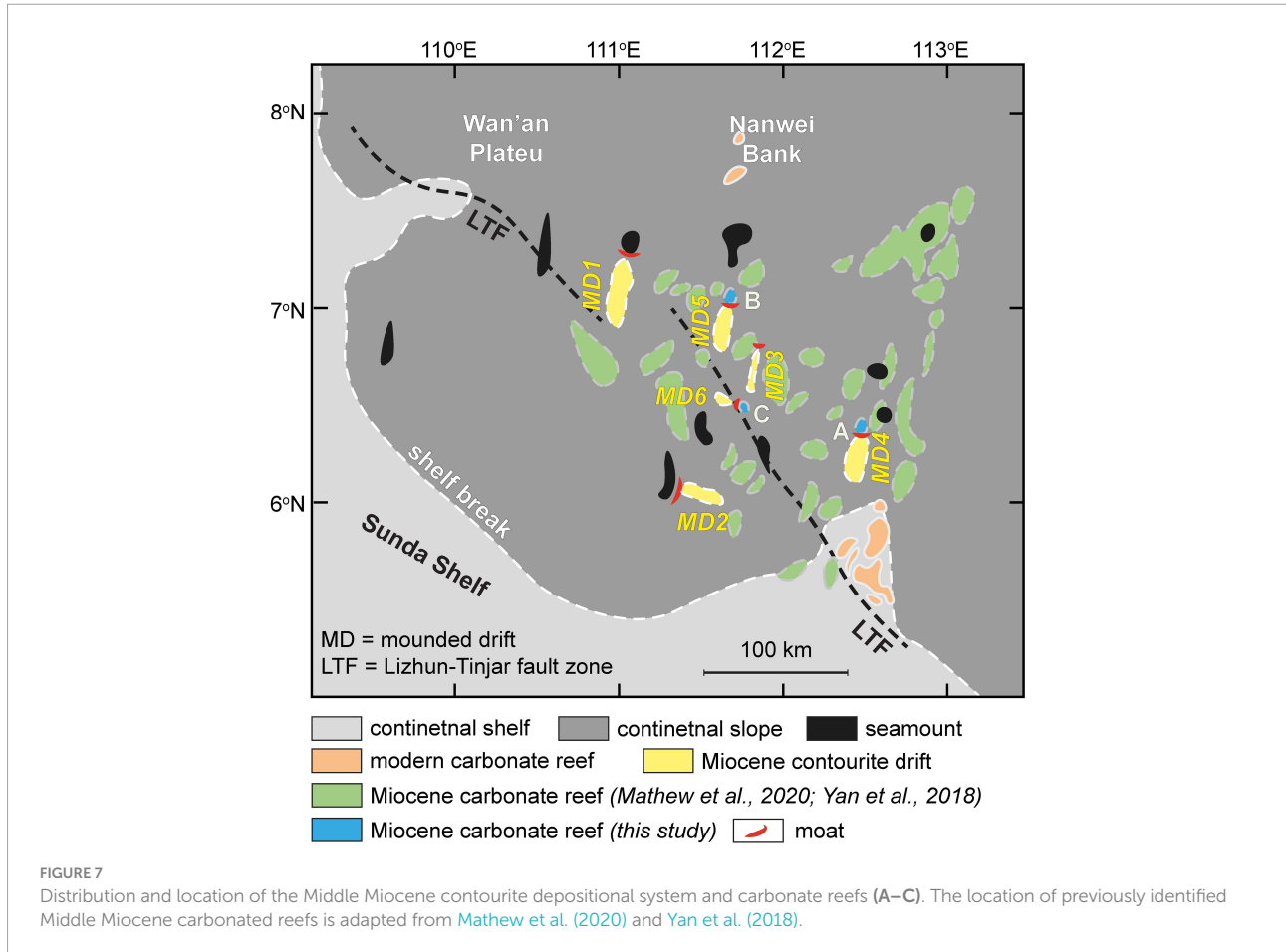
#### 5.1 Chronological framework

Discontinuities  $T_3$ ,  $T_2$ , and  $T_1$  of this study are correlated with previous chronostratigraphic interpretations of the southwest South China Sea (Figure 3C) (Madon et al., 2013; Luo et al., 2020; Huang et al., 2022). The correlation between seismic data and drill core data (Well Mulu-1 and Bako-1) shows that  $T_3$  corresponds to the Middle Miocene unconformity (MMU; 16 Ma).  $T_2$  marks

a transition of depositional styles from shallow water to deep marine, related to Wanan tectonic movement at 10.5 Ma, while  $T_1$  is correlated to Guangya tectonic movement at 5.3 Ma (Luo et al., 2020). Thus, UIII has a Middle Miocene age (16-10.5 Ma), UII a Late Miocene age (10.5-5.3 Ma), and UI a Pliocene-Quaternary age (<5.3 Ma) based on the chronostratigraphic constraints.

#### 5.2 Evolutionary stages of the contourite features

The major changes in the sedimentary stacking pattern and the outlined chronology of UIII, UII, and UI indicate three evolutionary stages of the contourite features: I) carbonate drift stage; II) burial stage; and III) modern stage (Figure 8). The carbonate drift stage reflects the growth of the Middle Miocene contourite depositional system between 16 and 10.5 Ma. The burial stage marks the terminated growth of carbonate drifts which are buried by the Late Miocene sedimentation during 10.5-5.3 Ma. The modern stage started with the development of Quaternary deep-water sedimentary systems since 5.3 Ma. These modern sedimentary systems are some of the major morphological features on the present-day seafloor in the study area.



### 5.2.1 Carbonate drift stage (16–10.5 Ma)

The carbonate drift stage (UIII) began with the growth of the Middle Miocene contourite drifts in the study area at 16 Ma (Figure 8A), coeval to the initial build-up of carbonate reefs on the Sunda Shelf in the southern South China Sea after ~18–15.5 Ma (Vahrenkamp et al., 2004; Mathew et al., 2020; Makhankova et al., 2021). Corals and foraminifera that constructed carbonate reefs on the proto-Sunda shelf indicated a shallow lagoon (<20 m depth) paleoenvironment during the Middle Miocene (Figure 3B) (Makhankova et al., 2021). The present-day continental slope south of the Nanwei Bank was used to be the outer continental shelf (50–200 m depth) during this period (Figure 9A) (Collins et al., 2018). Thus, the Middle Miocene contourite depositional system in UIII was generated in a shallow-marine setting.

Shallow-water contourite deposits can be shaped by bottom currents driven by four forces: 1) thermohaline circulation (Vandorpe et al., 2011); 2) wind-induced circulation (Nishida et al., 2022); 3) tidal flow (Lüdmann et al., 2013); and 4) processes at the water-mass interface (Verdicchio and Trincardi, 2008). For the reasons explained below, the Middle Miocene contourite depositional system in the study area was likely related to the wind-induced circulation.

The ocean circulation of the North Pacific enhanced and started to resemble the modern pattern after ~14 Ma (Nathan and Leckie, 2009; Kender et al., 2018). Surface waters had the possibility to intrude into the South China Sea because of its open connection with the Pacific (Figure 9A). However, the N-S thermocline gradient in the South China Sea only occurred after 11.5–10.6 Ma (Li et al., 2005; Jian et al., 2006). Contourite drifts in UIII were unlikely linked to the thermohaline circulation or processes at the water-mass interface because of the absence of stratified waters in the South China Sea during the Middle Miocene.

Sedimentary records on the Sunda Shelf showed a significant influence of tidal currents on the sediment deposition during the Middle Miocene (Koša, 2015; Amir Hassan et al., 2017). The related tidal currents were able to transport fine-grained sand and silt but were too weak to generate erosional features on the seafloor (Collins et al., 2017; Collins et al., 2018). Thus, tidal-induced circulation could hardly create moats in UIII and was not involved in the formation of the Middle Miocene contourite depositional system in the study area.

The Middle Miocene was also a significant period for the onset of the modern-like East Asian monsoon system (Betzler et al., 2016). The intensification of the East Asian monsoon at ~15–10 Ma greatly enhanced the seasonal wind-driven currents

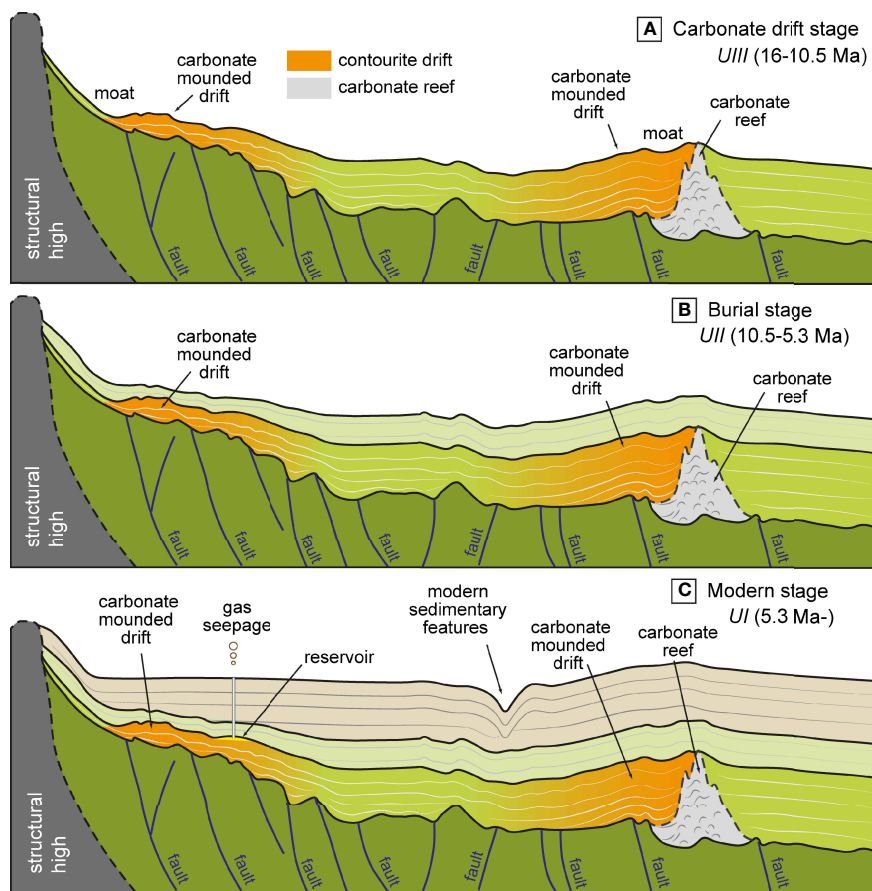


**FIGURE 8**  
Sketch of evolutionary stages of the contourite features in the southwest South China Sea: **(A)** Carbonate drift stage (16–10.5 Ma); **(B)** Burial stage (10.5–5.3 Ma); and **(C)** Modern Stage (5.3 Ma to present day).

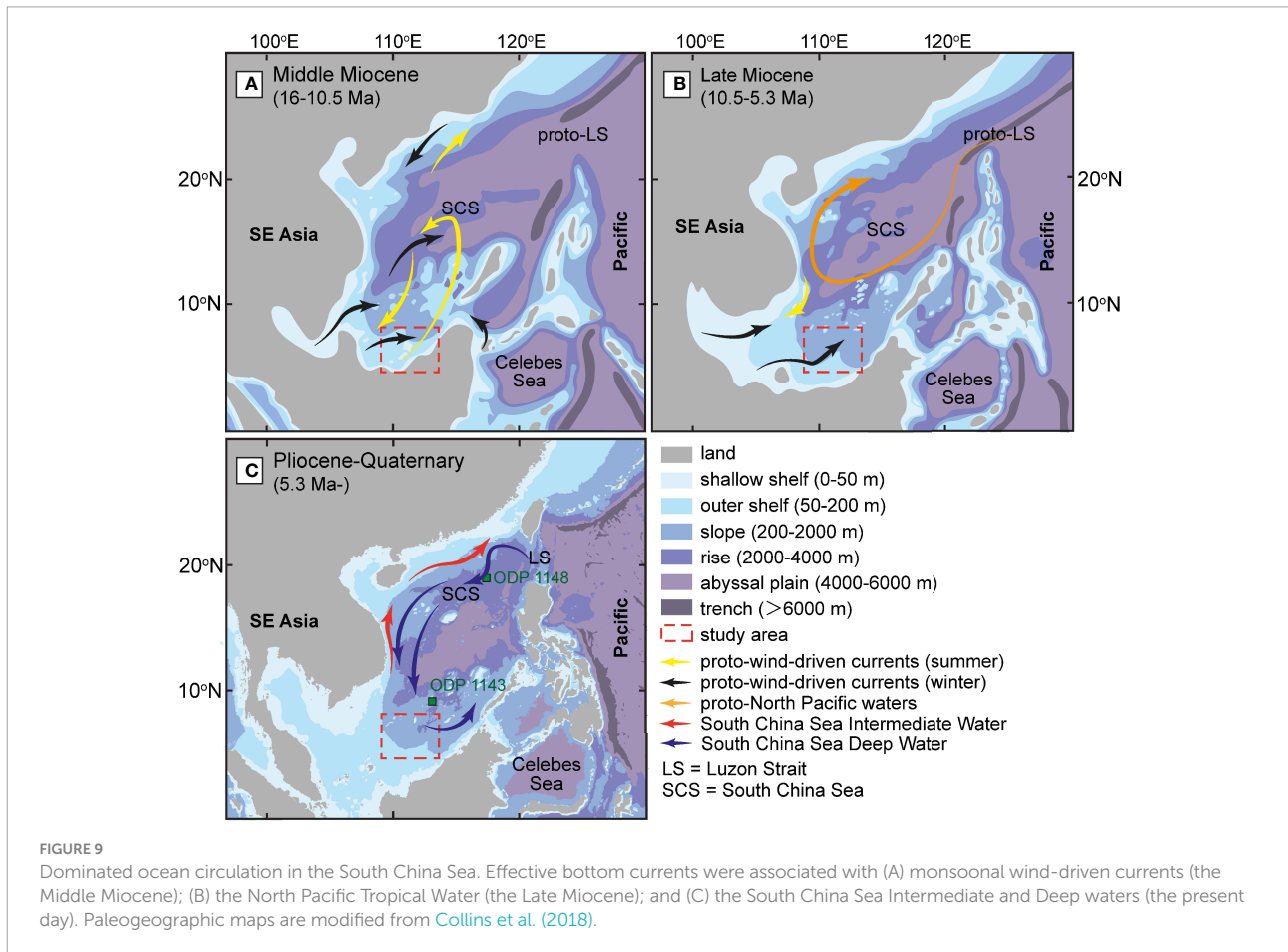
at the sea surface (Farnsworth et al., 2019; Holbourn et al., 2021; Ting et al., 2021). Siliciclastic materials were transported to the ocean, forming carbonate reefs and contourite drifts e.g., in the Maldives and on the proto-Sunda Shelf (Lüdmann et al., 2013; Betzler et al., 2016; Betzler et al., 2018). The W-E and NNE-SSW orientated moats in UIII in the study area indicate possible directions of wind-driven currents (Figure 10), which are comparable with the observation on the proto-Sunda Shelf (Ting et al., 2021). The reconstructed Middle Miocene wind-driven currents, resembled the modern pattern (Mathew et al., 2020; Ting et al., 2021), was namely flowed towards the north-northeast and the east during summer and winter monsoon in the study area (Figure 9A). Thus, wind-driven currents were responsible for the formation of the Middle Miocene contourite depositional system in UIII.

Notice that MD-3 and -6 only show at the lower part of UIII (Figures 5C and 6C). They were at a close distance and located at the Lizhun-Tinjar fault zone (Figure 7). The development of MD -3 and -6 was most likely hindered due to regional tectonic activities. Reactivation of the Lizhun-Tinjar

fault zone uplifted the paleo-seafloor and formed structural highs during the Middle Miocene (Liu et al., 2004). The resulted topographic barriers could profoundly change the pathway of oceanic currents (Gordon et al., 2003) and, in turn, control the development of contourite drifts.

### 5.2.2 Burial stage (10.5–5.3 Ma)

The burial stage (UII) of the contourite depositional system occurred between 10.5–5.3 Ma (Figure 8B). The contourite features became inactive and were buried by younger deposits after discontinuity  $T_2$  (Figures 5, 6). This prominent change in sedimentary stacking pattern was linked to variations in tectonics, paleoenvironment, and paleoceanography during the Late Miocene. Unlike the Middle Miocene tectonic uplift induced by the collision between the Nansha Islands (Dangerous Grounds) and the Borneo (Hutchison, 2004; Cullen, 2010; Ding et al., 2013), large-scale tectonics terminated at 10.5 Ma and rapid subsidence occurred in the southern South China Sea (Morley, 2016) (Figure 3A). The present-day continental slope



of the southwest South China Sea consequently transferred from shallow-marine to bathyal environments (Ding et al., 2013; Yan et al., 2020) (Figure 9B). Terrigenous clastic input greatly increased and most of the previously constructed carbonates reefs were drowned (Wu et al., 2016; Makhankova et al., 2021; Ting et al., 2021).

Wind-driven currents no longer influenced the deep seafloor in the study area, but stratified water masses persistently occupied the intermediate and deep layers of the southern South China Sea after 9.6 Ma (Li et al., 2005; Jian et al., 2006). Although the proto-North Pacific waters (NPW) influenced the South China Sea in an anticyclonic pattern during this time interval (Yin et al., 2021), the water mass flowed at the surface layer and could not create contourite features at the deeper site in the southwest South China Sea (Figure 9B).

### 5.2.3 Modern stage (<5.3 Ma)

The modern stage (UI) started with the generation of the present-day contourite drifts (Figure 10) (Liu et al., 2021). The modern-like ocean circulation was initiated after the establishment of the modern morphology of the Luzon Strait (Figure 9C) (Tian et al., 2017). The DW enters the study area with

a significant intensification in the velocity and generates numbers of contourite drifts and moats on the present-day seafloor (Liu et al., 2021).

## 5.3 Paleooceanographic implications

The evolution of the contourite depositional systems in the southwest South China Sea is compared with the contourite examples on other South China Sea margins (Figure 11). Changes in the South China Sea paleooceanography significantly influenced the sedimentary records along the water-mass pathways (Figure 11). The dominated bottom currents on sedimentary processes shifted from the monsoonal wind-driven currents to the NPW at 10.5 Ma and then the modern-like circulation system at 6.5–5.3 Ma (Figure 9).

The middle Miocene South China Sea was widely influenced by the monsoonal wind-driven currents (Figure 9A). The enhanced East Asian monsoon promoted surface currents (Farnsworth et al., 2019; Holbourn et al., 2021; Ting et al., 2021), which strongly shaped the morphology of the proto-continental shelves in the northern (Tian et al., 2015), the northwest (Zhuo

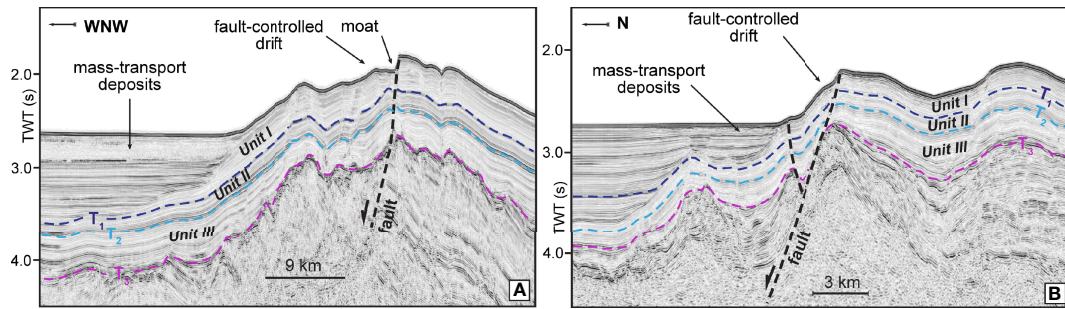


**FIGURE 10** Seismic profiles and their interpretation, showing present-day fault-controlled contourite drifts (Liu et al., 2021) and mass-transport deposits (He et al., 2018) in the seismic unit I. The location of these seismic lines is displayed in Figure 1B. Discontinuities  $T_3$  (16 Ma; purple dotted line),  $T_2$  (10.5 Ma; light blue dotted line), and  $T_1$  (5.3 Ma; dark blue dotted line) are indicated.

et al., 2014), and the southwest South China Sea. The related wind-driven currents created mounded contourite features in the Xisha region (Tian et al., 2015), the Zhongjian basin (Yang et al., 2021) and the study area (Figure 11). The development of these contourite features terminated at 10.5 Ma.

After 10.6 Ma, the latitudinal thermocline gradient firstly appeared in the South China Sea (Jian et al., 2006), coinciding with the intrusion of the proto-NPW (Yin et al., 2021). The monsoonal wind-driven currents only created contourite features on the proto-Sunda Shelf in the southwest South China Sea (Mathew et al., 2020), while the proto-NPW profoundly influenced the western (Yin et al., 2021) and northwest (Palamenghi et al., 2015), and northern margins (Wang et al., 2022) in the South China Sea during the Late Miocene (Figure 9B). The external shape of these contourite drifts varied from mounded (Palamenghi et al., 2015; Yin et al., 2021) to sheeted geometry (Wang et al., 2022) towards the distal site of the proto-NPW pathway. The proto-NPW would gradually lose the energy towards the northern South China Sea as the sheeted drifts are shaped by weak bottom currents (Faugères et al., 1999; Hernández-Molina et al., 2008; Rebesco et al., 2014).

Benthic foraminiferal  $\delta^{18}O$  and  $\delta^{13}C$  of ODP Sites 1143 and 1148 have indicated significant changes in the South China Sea paleoceanography at 6.5 Ma (Figure 11) (Li et al., 2006; Tian et al., 2017), coeval with the initial isolation of the South China Sea (Chen et al., 2015; Tian et al., 2017; Huang et al., 2018). The sandwich-like (inflow-outflow-inflow) water mass exchange was initiated through the Luzon Strait (Chen et al., 2015; Yin et al., 2021). The present-day anticyclonic IW (Tian et al., 2006) and cyclonic DW (Qu et al., 2006) were consequently formed in the South China Sea (Figure 9C), generating contourite depositional systems along IW and DW pathways from the latest Miocene onwards (Figure 11) (Palamenghi et al., 2015; Chen et al., 2016; Wang et al., 2018; Chen et al., 2019; Chen et al., 2021; Liu et al., 2021; Yin et al., 2021).

### 5.4 Economic implications

Shallow-water contourite drifts in UIII are served as a good gas reservoir in the study area. The fluid-escape pipe that is

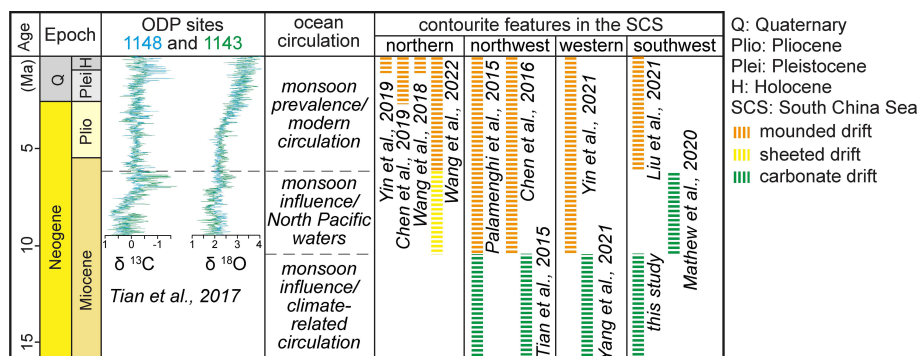


**FIGURE 11** The formation time and distribution of contourite features in the South China Sea since the Middle Miocene. Dominated oceanic circulation and paleoceanography are indicated. The location of ODP sites 1148 and 1143 is shown in Figure 9C.

deeply rooted at the mounded drift 3 extended to the seafloor and formed a pockmark (Figure 5C). The core CL49 acquired at the pockmark shows intense methane leakage from the fluid-escape pipe (Table 1), indicating sufficient hydrocarbon fluid sources in the deep part of seismic units (Huang et al., 2022). Previous studies demonstrated that the deformed seismic unit below  $T_3$  (in Figure 5) was the Eocene to Late Miocene source rocks (Zhang et al., 2017). They contained mixed Type II/III kerogen and potentially supplied  $1.4855 \times 10^{12} \text{ m}^3$  natural gas in the study area (Zhang et al., 2017; Lei et al., 2019; Tang et al., 2021). Therefore, natural gas was likely migrated upwards from the deformed unit via previously documented faults (Figure 3C) (e.g., Lei et al., 2019; Luo et al., 2020) and then reserved in buried contourite drifts in UIII.

The true lithology of these shallow-water contourite drifts in UIII is unknown because of the limited dataset. However, they were most likely coarse-grained and poorly sorted. Shallow-water contourite drifts in UIII were generated in adjacent or associated with carbonate reefs in the study area (Figure 7). Such contourite deposits are directly sourced from the adjacent reefs and composed of coarse-grained carbonate sands (Lüdmann et al., 2013; Chabaud et al., 2016; Eberli and Betzler, 2019). Coarse-grained carbonate drifts are potential hydrocarbon reservoirs because of their high porosity, high permeability, and effective lateral and vertical transmissibility of fluids (Viana, 2008). Similar examples were observed in the eastern Gulf of Cádiz (León et al., 2014), the western Alborán Sea (Somoza et al., 2012; León et al., 2014), and the mid-Norwegian margin (Hustoft et al., 2010; Plaza-Faverola et al., 2010), where fluid flow escaped from the coarse-grained contourite layers and caused natural gas leakage. Similarities between these contourite examples indicate the great economic potential of the Middle Miocene carbonate contourite drifts in the southwest South China Sea.

TABLE 1 Hydrocarbon components and carbon isotope values of the methane in core CL49 (Huang et al., 2022).

Interval(mbsf)	Methane (ppm)	Propane (ppm)	$C_1/C_{2+}$ ratio
0.5–0.6	23.9	0.45	23.7
1.1–1.2	23.0	0.38	60.5
1.7–1.8	24.2	0.41	59.0
2.3–2.4	22.4	0.36	62.2
2.9–3.0	22.9	0.52	11.3
3.5–3.6	21.7	0.34	63.8
4.1–4.2	21.6	0.52	17.9
4.7–4.8	22.8	0.41	25.9
5.3–5.4	19.1	0.23	83.0
5.9–6.0	22.6	–	–
6.5–6.6	1298	–	–
7.1–7.2	1249	–	–

## 6 Conclusion

This study demonstrates the previously undocumented occurrence of carbonate contourite drifts in the southwest South China Sea. Analysis of seismic reflection data and previously established chronology allows the identification of the Middle Miocene contourite depositional system. The distribution, characteristics, and evolution of the contourite features have significant sedimentary, paleoceanographic, and economic implications:

- Three evolutionary phases are identified for the contourite drifts' construction: I) a carbonate drift stage (16–10.5 Ma) where six carbonate contourite drifts were built by the monsoonal wind-driven currents; II) a burial stage (10.5–5.3 Ma) where contourite features became inactive and were buried by younger deposits; and III) a modern stage from the 5.3 Ma till the present-day, characterized by the modern contourite features associated with the South China Sea Deep Water;
- The dominated bottom currents in the South China Sea shifted from the monsoonal wind-driven currents to the North Pacific waters at 10.5 Ma and then the modern circulation system at 6.5–5.3 Ma. The paleoceanographic changes significantly influenced the sedimentary records along the water-mass pathways in the South China Sea.
- Shallow-water carbonate contourite drifts are good gas reservoirs. They were generated in adjacent or associated with carbonate reefs during the Middle Miocene. The drifts were possibly composed of coarse-grained carbonate sands. Fluid flow escaped from the coarse-grained contourite layers and caused intense methane leakage on the seafloor.

## Data availability statement

The oceanographic data of this study are available in the World Ocean Database (2013) (<https://www.nodc.noaa.gov/OC5/WOD13>). Seismic profiles and bathymetric data acquired by the China Geological Survey are not publicly available due to privacy or ethical restrictions. Requests to access these datasets should be directed to ZLe, 44231234@qq.com.

## Author contributions

SL wrote the manuscript and interpreted all the datasets. MS, Zli, and BZ interpreted the bathymetry data and seismic profiles. ZLe was involved in the acquisition and processing of the seismic profiles. HS took part in the geomorphological interpretation. All authors contributed to the article and approved the submitted version.

## Funding

This study was supported by the China Postdoctoral Science Foundation (NO. 2020TQ0369 and NO. 2021M703668). This study was carried out within the framework of the Geological Investigation Programs (No. DD20160155) of the China Geological Survey. The study was also supported by Southern Marine Science and Engineering Guangdong Laboratory (Zhuhai) (No. SML2021SP307).

## Acknowledgments

The authors wish to thank all crews and scientific researchers participated in the R/V Tanbao cruise in 1996, 2009, and 2013 during the acquisition of bathymetric and seismic datasets. The authors also thanks Dr. Haiteng Zhuo and Dr. Qin Yongpeng

## References

- Amir Hassan, M. H., Johnson, H. D., Allison, P. A. and Abdullah, W. H. (2017). *Sedimentology and stratigraphic architecture of a Miocene retrogradational, tide-dominated delta system: Balingian province, offshore Sarawak, Malaysia* Vol. 444 (London: Geological Society), 215. Special Publications. doi: 10.1144/SP444.12
- Banerjee, A. and Ahmed Salim, A. M. (2021). Stratigraphic evolution of deep-water dangerous grounds in the south China Sea, NW sabah platform region, Malaysia. *J. Petroleum Sci. Eng.* 201, 108434. doi: 10.1016/j.petrol.2021.108434
- Barckhausen, U. and Roeser, H. A. (2004). "Seafloor spreading anomalies in the south China Sea revisited," in *Continent-ocean interactions within East Asian marginal seas*, eds. P. Clift, W. Kuhnt, P. Wang, and D. Hayes (Washington DC, USA: American Geophysical Union), 121–125.
- Betzler, C., Eberli, G. P., Kroon, D., Wright, J. D., Swart, P. K., Nath, B. N., et al. (2016). The abrupt onset of the modern south Asian monsoon winds. *Sci. Rep.* 6 (1), 29838. doi: 10.1038/srep29838
- Betzler, C., Eberli, G. P., Lüdmann, T., Reolid, J., Kroon, D., Reijmer, J. J. G., et al. (2018). Refinement of Miocene sea level and monsoon events from the sedimentary archive of the Maldives (Indian ocean). *Prog. Earth Planetary Sci.* 5 (1), 5. doi: 10.1186/s40645-018-0165-x
- Betzler, C., Lindhorst, S., Eberli, G. P., Lüdmann, T., Möbius, J., Ludwig, J., et al. (2014). Periplatform drift: The combined result of contour current and off-bank transport along carbonate platforms. *Geology* 42 (10), 871–874. doi: 10.1130/g35900.1
- Boyer, T. P., Antonov, J. I., Baranova, O. K., Garcia, H. E., Johnson, D. R., Mishonov, A. V., et al. (2013). *World ocean database 2013*. doi: 10.7289/V5NZ85MT
- Burgess, P. M., Winefield, P., Minzoni, M. and Elders, C. (2013). *Methods for identification of isolated carbonate buildups from seismic reflection data*. Am Assoc Pet Geol Bul. (AAPG Bulletin), 97 1071–1098. doi: 10.1306/12051212011
- Catuneanu, O., Abreu, V., Bhattacharya, J. P., Blum, M. D., Dalrymple, R. W., Eriksson, P. G., et al. (2009). Towards the standardization of sequence stratigraphy. *Earth-Science Rev.* 92 (1), 1–33. doi: 10.1016/j.earscirev.2008.10.003
- Ceramicola, S., Rebesco, M., De Batist, M. and Khlystov, O. (2001). Seismic evidence of small-scale lacustrine drifts in lake baikal (Russia). *Mar. Geophysical Res.* 22 (5), 445–464. doi: 10.1023/a:1016351700435
- Chabaud, L., Ducassou, E., Tournadour, E., Mulder, T., Reijmer, J. J. G., Conesa, G., et al. (2016). Sedimentary processes determining the modern carbonate periplatform drift of little bahama bank. *Mar. Geology* 378, 213–229. doi: 10.1016/j.margeo.2015.11.006
- Chang, S.-P., Pubellier, M., Descluse, M., Qiu, Y., Nirrengarten, M., Mohn, G., et al. (2022). Crustal architecture and evolution of the southwestern south China Sea: Implications to continental breakup. *Mar. Petroleum Geology* 136, 105450. doi: 10.1016/j.marpetgeo.2021.105450
- Chen, W.-H., Huang, C.-Y., Lin, Y.-J., Zhao, Q., Yan, Y., Chen, D., et al. (2015). Depleted deep south China Sea  $\delta^{13}C$  paleoceanographic events in response to tectonic evolution in Taiwan–Luzon strait since middle Miocene. *Deep Sea Res. Part II: Topical Stud. Oceanography* 122, 195–225. doi: 10.1016/j.dsr2.2015.02.005
- Chen, H., Xie, X., Zhang, W., Shu, Y., Wang, D., Vandorpe, T., et al. (2016). Deep-water sedimentary systems and their relationship with bottom currents at the intersection of xisha trough and Northwest Sub-basin, south China Sea. *Mar. Geology* 378, 101–113. doi: 10.1016/j.margeo.2015.11.002
- Chen, H., Zhang, W., Xie, X., Gao, Y., Liu, S., Ren, J., et al. (2021). Linking oceanographic processes to contourite features: Numerical modelling of currents influencing a contourite depositional system on the northern south China Sea margin. *Mar. Geology* 444, 106714. doi: 10.1016/j.margeo.2021.106714
- Chen, H., Zhang, W., Xie, X. and Ren, J. (2019). Sediment dynamics driven by contour currents and mesoscale eddies along continental slope: A case study of the northern south China Sea. *Mar. Geology* 409, 48–66. doi: 10.1016/j.margeo.2018.12.012
- Cimino, M. A., Santora, J. A., Schroeder, I., Sydeman, W., Jacox, M. G., Hazen, E. L., et al. (2020). Essential krill species habitat resolved by seasonal upwelling and ocean circulation models within the large marine ecosystem of the California current system. *Ecography* 43 (10), 1536–1549. doi: 10.1111/ecog.05204
- Collins, D. S., Avdis, A., Allison, P. A., Johnson, H. D., Hill, J. and Piggott, M. D. (2018). Controls on tidal sedimentation and preservation: Insights from numerical tidal modelling in the late oligocene–Miocene south China Sea, southeast Asia. *Sedimentology* 65 (7), 2468–2505. doi: 10.1111/sed.12474
- Collins, D. S., Avdis, A., Allison, P. A., Johnson, H. D., Hill, J., Piggott, M. D., et al. (2017). Tidal dynamics and mangrove carbon sequestration during the oligo–Miocene in the south China Sea. *Nat. Commun.* 8 (1), 15698. doi: 10.1038/ncomms15698
- Cullen, A. B. (2010). Transverse segmentation of the baram-balabac basin, NW Borneo: refining the model of borneos tectonic evolution. *Petroleum Geosci.* 16 (1), 3. doi: 10.1144/1354-079309-828
- de Castro, S., Hernández-Molina, F. J., de Weger, W., Jiménez-Espejo, F. J., Rodríguez-Tovar, F. J., Mena, A., et al. (2021). Contourite characterization and its discrimination from other deep-water deposits in the gulf of cadiz contourite depositional system. *Sedimentology* 68 (3), 987–1027. doi: 10.1111/sed.12813
- de Weger, W., Hernández-Molina, F. J., Flecker, R., Sierro, F. J., Chiarella, D., Krijgsman, W., et al. (2020). Late Miocene contourite channel system reveals intermittent overflow behavior. *Geology* 48 (12), 1194–1199. doi: 10.1130/G47944.1
- Ding, W., Franke, D., Li, J. and Steuer, S. (2013). Seismic stratigraphy and tectonic structure from a composite multi-channel seismic profile across the entire dangerous grounds, south China Sea. *Tectonophysics* 582, 162–176. doi: 10.1016/j.tecto.2012.09.026

for their valuable suggestions, which have greatly improved this manuscript.

## Conflict of interest

The authors declare that the research was conducted in the absence of any commercial or financial relationships that could be construed as a potential conflict of interest.

## Publisher's note

All claims expressed in this article are solely those of the authors and do not necessarily represent those of their affiliated organizations, or those of the publisher, the editors and the reviewers. Any product that may be evaluated in this article, or claim that may be made by its manufacturer, is not guaranteed or endorsed by the publisher.

- Eberli, G. P. and Betzler, C. (2019). Characteristics of modern carbonate contourite drifts. *Sedimentology* 66 (4), 1163–1191. doi: 10.1111/sed.12584
- Farnsworth, A., Lunt Daniel, J., Robinson Stuart, A., Valdes Paul, J., Roberts William, H. G., Clift Peter, D., et al. (2019). *Past East Asian monsoon evolution controlled by paleogeography, not CO<sub>2</sub>* (eaa1697: Science Advances 5(10). doi: 10.1126/sciadv.aax1697
- Faugères, J. C. and Stow, D. A. V. (2008). “Chapter 14 contourite drifts: Nature, evolution and controls,” in *Developments in sedimentology*, vol. 257–288. Eds. Rebesco, M. and Camerlenghi, A. (Amsterdam, NL: Elsevier).
- Faugères, J.-C., Stow, D. A. V., Imbert, P. and Viana, A. (1999). Seismic features diagnostic of contourite drifts. *Mar. Geology* 162 (1), 1–38. doi: 10.1016/S0025-3227(99)00068-7
- García, M., Lobo, F. J., Maldonado, A., Hernández-Molina, F. J., Bohoyo, F. and Pérez, L. F. (2016). High-resolution seismic stratigraphy and morphology of the scan basin contourite fan, southern Scotia Sea, Antarctica. *Mar. Geology* 378, 361–373. doi: 10.1016/j.margeo.2016.01.011
- Gordon, A. L., Giulivi, C. F. and Ilahude, A. G. (2003). Deep topographic barriers within the Indonesian seas. *Deep Sea Res. Part II: Topical Stud. Oceanography* 50 (12), 2205–2228. doi: 10.1016/S0967-0645(03)00053-5
- Hall, R. (2002). Cenozoic Geological and plate tectonic evolution of SE Asia and the SW Pacific: computer-based reconstructions, model and animations. *J. Asian Earth Sci.* 20 (4), 353–431. doi: 10.1016/S1367-9120(01)00069-4
- Hanebuth, T. J. J., Zhang, W., Hofmann, A. L., Lowemark, L. A. and Schwenk, T. (2015). Oceanic density fronts steering bottom-current induced sedimentation deduced from a 50 ka contourite-drift record and numerical modeling (off NW Spain). *Quaternary Sci. Rev.* 112, 207–225. doi: 10.1016/j.quascirev.2015.01.027
- Heezen, B. C. and Hollister, C. (1964). Deep-sea current evidence from abyssal sediments. *Mar. Geology* 1 (2), 141–174. doi: 10.1016/0025-3227(64)90012-X
- Heezen, B. C., Hollister, C. D. and Ruddiman, W. F. (1966). Shaping of the continental rise by deep geostrophic contour currents. *Science* 152(3721), 502. doi: 10.1126/science.152.3721.502
- He, Y., Kuang, Z. and Xu, M. (2018) Seismic reflection characteristics and triggering mechanism of mass transport deposits of Quaternary in Beikang Basin, Geological Science and Technology Information. 37 (4), 258–268. doi: 10.19509/j.cnki.dzqk.2018.0435.
- Hendry, J., Burgess, P., Hunt, D., Janson, X. and Zampetti, V. (2021). *Seismic characterization of carbonate platforms and reservoirs: an introduction and review* Vol. 509 (London: Geological Society), 1. Special Publications. doi: 10.1144/SP509-2021-51
- Hernández-Molina, F. J., Campbell, S., Badalini, G., Thompson, P., Walker, R., Soto, M., et al. (2017). Large Bedforms on contourite terraces: Sedimentary and conceptual implications. *Geology* 46 (1), 27–30. doi: 10.1130/G39655.1
- Hernández-Molina, F. J., Llave, E. and Stow, D. A. V. (2008). Chapter 19 Continental Slope Contourites,” in *Developments Sedimentology*, eds. M. Rebesco and A. Camerlenghi. (Amsterdam, NL: Elsevier), 379–408. doi: 10.1016/S0070-4571(08)10019-X
- Hernández-Molina, F. J., Sierro, F. J., Llave, E., Roque, C., Stow, D. A. V., Williams, T., et al. (2016). Evolution of the gulf of cadiz margin and southwest Portugal contourite depositional system: Tectonic, sedimentary and paleoceanographic implications from IODP expedition 339. *Mar. Geology* 377, 7–39. doi: 10.1016/j.margeo.2015.09.013
- Holbourn, A., Kuhnt, W., Clemens, S. C. and Heslop, D. (2021). A ~12 myr Miocene record of East Asian monsoon variability from the south China Sea. *Paleoceanography Paleoclimatology* 36 (7), e2021PA004267. doi: 10.1029/2021PA004267
- Howe, J. A., Stoker, M. S., Masson, D. G., Pudsey, C. J., Morris, P., Larter, R. D., et al. (2006). Seabed morphology and the bottom-current pathways around rosemary bank seamount, northern rockall trough, north Atlantic. *Mar. Petroleum Geology* 23 (2), 165–181. doi: 10.1016/j.marpetgeo.2005.08.003
- Huang, C.-Y., Chen, W.-H., Wang, M.-H., Lin, C.-T., Yang, S., Li, X., et al. (2018). Juxtaposed sequence stratigraphy, temporal-spatial variations of sedimentation and development of modern-forming forearc lichi mélange in north Luzon trough forearc basin onshore and offshore eastern Taiwan: An overview. *Earth-Science Rev.* 182, 102–140. doi: 10.1016/j.earscirev.2018.01.015
- Huang, W., Meng, M., Zhang, W., Shang, J., Liang, J., Wan, Z., et al. (2022). Geological, geophysical, and geochemical characteristics of deep-routed fluid seepage and its indication of gas hydrate occurrence in the beikang basin, southern south China Sea. *Mar. Petroleum Geology* 139, 105610. doi: 10.1016/j.marpetgeo.2022.105610
- Hustoft, S., Bünz, S. and Mienert, J. (2010). Three-dimensional seismic analysis of the morphology and spatial distribution of chimneys beneath the nyegga pockmark field, offshore mid-Norway. *Basin Res.* 22 (4), 465–480. doi: 10.1111/j.1365-2117.2010.00486.x
- Hutchison, C. S. (2004). Marginal basin evolution: the southern south China Sea. *Mar. Petroleum Geology* 21 (9), 1129–1148. doi: 10.1016/j.marpetgeo.2004.07.002
- Jian, Z., Yu, Y., Li, B., Wang, J., Zhang, X. and Zhou, Z. (2006). Phased evolution of the south–north hydrographic gradient in the south China Sea since the middle Miocene. *Paleogeography Palaeoclimatology Palaeoecol.* 230 (3), 251–263. doi: 10.1016/j.palaeo.2005.07.018
- Kane, I. A. and Clare, M. A. (2019). Dispersion, accumulation, and the ultimate fate of microplastics in deep-marine environments: A review and future directions. *Front. Earth Sci.* 7 (80). doi: 10.3389/feart.2019.00080
- Kender, S., Bogus, K. A., Cobb, T. D. and Thomas, D. J. (2018). Neodymium evidence for increased circumpolar deep water flow to the north Pacific during the middle Miocene climate transition. *Paleoceanography Paleoclimatology* 33 (7), 672–682. doi: 10.1029/2017PA003309
- Kirby, A., Hernández-Molina, F. J., Rodriguez, P. and Conti, B. (2021). Sedimentary stacking pattern of plastered drifts: An example from the Cenozoic on the Uruguayan continental slope. *Mar. Geology* 440, 106567. doi: 10.1016/j.margeo.2021.106567
- Koša, E. (2015). Sea-Level changes, shoreline journeys, and the seismic stratigraphy of central luconia, Miocene-present, offshore Sarawak, NW Borneo. *Mar. Petroleum Geology* 59, 35–55. doi: 10.1016/j.marpetgeo.2014.07.005
- Lei, Z.-y., Zhang, L., Su, M. and Qian, X. (2019). Types, characteristics and implication for hydrocarbon exploration of the middle Miocene deep-water sediments in beikang basin, southern south China Sea. *China Geology* 2 (1), 85–93. doi: 10.31035/cg2018094
- León, R., Somoza, L., Medialdea, T., González, F. J., Gimenez-Moreno, C. J. and Pérez-López, R. (2014). Pockmarks on either side of the strait of Gibraltar: formation from overpressured shallow contourite gas reservoirs and internal wave action during the last glacial sea-level lowstand? *Geo-Marine Lett.* 34 (2), 131–151. doi: 10.1007/s00367-014-0358-2
- Li, B., Jian, Z., Li, Q., Tian, J. and Wang, P. (2005). Paleoceanography of the south China Sea since the middle Miocene: evidence from planktonic foraminifera. *Mar. Micropaleontology* 54 (1), 49–62. doi: 10.1016/j.marmicro.2004.09.003
- Liu, S., Hernández-Molina, F. J., Lei, Z., Duarte, D., Chen, H., Wang, C., et al. (2021). Fault-controlled contourite drifts in the southern south China Sea: Tectonic, oceanographic, and conceptual implications. *Mar. Geology* 433, 106420. doi: 10.1016/j.margeo.2021.106420
- Liu, H.-l., Yan, P., Zhang, B.-y., Sun, Y., Zhang, Y.-x., Shu, L.-s., et al. (2004). Role of the wan-Na fault system in the western nansha islands (Southern south China Sea). *J. Asian Earth Sci.* 23 (2), 221–233. doi: 10.1016/S1367-9120(03)00121-4
- Li, Q., Wang, P., Zhao, Q., Shao, L., Zhong, G., Tian, J., et al. (2006). A 33 ma lithostratigraphic record of tectonic and paleoceanographic evolution of the south China Sea. *Mar. Geology* 230 (3), 217–235. doi: 10.1016/j.margeo.2006.05.006
- Li, G., Xu, W., Luo, Y., Liu, J., Zhao, J., Feng, Y., et al. (2022). *Strontium isotope stratigraphy and LA-ICP-MS U-Pb carbonate age constraints on the Cenozoic tectonic evolution of the southern south China Sea* (Geol Soc Am Bull). doi: 10.1130/b36365.1
- Llave, E., Hernández-Molina, F. J., Stow, D. A. V., Fernández-Puga, M. C., García, M., Vázquez, J. T., et al. (2007). Reconstructions of the Mediterranean outflow water during the quaternary based on the study of changes in buried mounded drift stacking pattern in the gulf of cadiz. *Mar. Geophysical Res.* 28 (4), 379–394. doi: 10.1007/s11001-007-9040-7
- Loeb, V., Hofmann, E. E., Klinck, J. M. and Holm-Hansen, O. (2010). Hydrographic control of the marine ecosystem in the south Shetland-elephant island and bransfield strait region. *Deep Sea Res. Part II: Topical Stud. Oceanography* 57 (7), 519–542. doi: 10.1016/j.dsr2.2009.10.004
- Lüdmann, T., Kalvelage, C., Betzler, C., Fürstenau, J. and Hübscher, C. (2013). The Maldives, a giant isolated carbonate platform dominated by bottom currents. *Mar. Petroleum Geology* 43, 326–340. doi: 10.1016/j.marpetgeo.2013.01.004
- Luo, S., Wang, X., Zhang, L., Lei, Z. and Shuai, Q. (2020). Study of high-quality sandstone in early Miocene sequence of beikang-zengmu basin, the southern south China Sea. *Mar. Geology Quaternary Geology* 40 (2), 111–123. doi: 10.16562/j.cnki.0256-1492.2018122601
- Madon, M., Kim, C. L. and Wong, R. (2013). The structure and stratigraphy of deepwater Sarawak, Malaysia: Implications for tectonic evolution. *J. Asian Earth Sci.* 76, 312–333. doi: 10.1016/j.jseas.2013.04.040
- Magee, C., Hunt-Stewart, E. and Jackson, C. A. L. (2013). Volcano growth mechanisms and the role of sub-volcanic intrusions: Insights from 2D seismic reflection data. *Earth Planetary Sci. Lett.* 373, 41–53. doi: 10.1016/j.epsl.2013.04.041
- Makhankova, A., Sautter, B., Mathew, M., Menier, D. and Poppelreiter, M. (2021). Seismic stratigraphy and sedimentology of a Miocene carbonate platform in luconia, south China Sea. *Geological J.* 56 (1), 1–17. doi: 10.1002/gj.3942

- Martin, J., Lusher, A., Thompson, R. C. and Morley, A. (2017). The deposition and accumulation of microplastics in marine sediments and bottom water from the Irish continental shelf. *Sci. Rep.* 7 (1), 10772. doi: 10.1038/s41598-017-11079-2
- Mathew, M., Makhankova, A., Menier, D., Sautter, B., Betzler, C. and Pierson, B. (2020). The emergence of Miocene reefs in south China Sea and its resilient adaptability under varying eustatic, climatic and oceanographic conditions. *Sci. Rep.* 10 (1), 7141. doi: 10.1038/s41598-020-64119-9
- Morley, C. K. (2002). A tectonic model for the tertiary evolution of strike-slip faults and rift basins in SE Asia. *Tectonophysics* 347 (4), 189–215. doi: 10.1016/S0040-1951(02)00061-6
- Morley, C. K. (2016). Major unconformities/termination of extension events and associated surfaces in the south China seas: Review and implications for tectonic development. *J. Asian Earth Sci.* 120, 62–86. doi: 10.1016/j.jseas.2016.01.013
- Mulder, T., Ducassou, E., Hanquiez, V., Principaud, M., Fauquembergue, K., Tournadour, E., et al. (2019). Contour current imprints and contourite drifts in the Bahamian archipelago. *Sedimentology* 66 (4), 1192–1221. doi: 10.1111/sed.12587
- Nathan, S. A. and Leckie, R. M. (2009). Early history of the Western Pacific warm pool during the middle to late Miocene (~13.2–5.8 ma): Role of sea-level change and implications for equatorial circulation. *Palaeogeography Palaeoclimatology Palaeoecol.* 274 (3), 140–159. doi: 10.1016/j.palaeo.2009.01.007
- Ng, Z. L., Hernández-Molina, F. J., Duarte, D., Roque, C., Sierro, F. J., Llave, E., et al. (2021). Late Miocene contourite depositional system of the gulf of cádiz: The sedimentary signature of the paleo-Mediterranean outflow water. *Mar. Geology* 442, 106605. doi: 10.1016/j.margeo.2021.106605
- Nishida, N., Itaki, T., Amano, A., Katayama, H., Sato, T., Stow, D., et al. (2022). Anatomy and dynamics of a mixed contourite sand sheet, Ryukyu island arc, northwestern Pacific ocean. *Mar. Geology* 444, 106707. doi: 10.1016/j.margeo.2021.106707
- Palamenghi, L., Keil, H. and Spiess, V. (2015). Sequence stratigraphic framework of a mixed turbidite-contourite depositional system along the NW slope of the south China Sea. *Geo-Marine Lett.* 35 (1), 1–21. doi: 10.1007/s00367-014-0385-z
- Pepe, F., Di Donato, V., Insinga, D., Molisso, F., Faraci, C., Sacchi, M., et al. (2018). Seismic stratigraphy of upper quaternary shallow-water contourite drifts in the gulf of taranto (Ionian Sea, southern Italy). *Mar. Geology* 397, 79–92. doi: 10.1016/j.margeo.2017.12.004
- Pérez, L. F., Hernández-Molina, F. J., Lodolo, E., Bohoyo, F., Galindo-Zaldívar, J. and Maldonado, A. (2019). Oceanographic and climatic consequences of the tectonic evolution of the southern scotia sea basins, Antarctica. *Earth-Science Rev.* 198, 102922. doi: 10.1016/j.earscirev.2019.102922
- Plaza-Faverola, A., Bünz, S. and Mienert, J. (2010). Fluid distributions inferred from p-wave velocity and reflection seismic amplitude anomalies beneath the nyegga pockmark field of the mid-Norwegian margin. *Mar. Petroleum Geology* 27 (1), 46–60. doi: 10.1016/j.marpetgeo.2009.07.007
- Qu, T., Girton, J. B. and Whitehead, J. A. (2006). Deepwater overflow through Luzon strait. *J. Geophysical Research: Oceans* 111, C01002. doi: 10.1029/2005JC003139
- Qu, T., Song, Y. T. and Yamagata, T. (2009). An introduction to the south China Sea throughflow: Its dynamics, variability, and application for climate. *Dynamics Atmospheres Oceans* 47 (1), 3–14. doi: 10.1016/j.dynatmoce.2008.05.001
- Rebesco, M., Hernández-Molina, F. J., Van Rooij, D. and Wählin, A. (2014). Contourites and associated sediments controlled by deep-water circulation processes: State-of-the-art and future considerations. *Mar. Geology* 352, 111–154. doi: 10.1016/j.margeo.2014.03.011
- Rodrigues, S., Hernández-Molina, F. J., Hillenbrand, C. D., Lucchi, R. G., Rodríguez-Tovar, F. J., Rebesco, M., et al. (2022). Recognizing key sedimentary facies and their distribution in mixed turbidite-contourite depositional systems: The case of the Pacific margin of the Antarctic peninsula. *Sedimentology*. 69, 1953–1991. doi: 10.1111/sed.12978
- Roque, C., Duarte, H., Terrinha, P., Valadares, V., Noiva, J., Cachão, M., et al. (2012). Pliocene and quaternary depositional model of the Algarve margin contourite drifts (Gulf of cádiz, SW Iberia): Seismic architecture, tectonic control and paleoceanographic insights. *Mar. Geology* 303–306, 42–62. doi: 10.1016/j.margeo.2011.11.001
- Sibuet, J.-C., Yeh, Y.-C. and Lee, C.-S. (2016). Geodynamics of the south China Sea. *Tectonophysics* 692, 98–119. doi: 10.1016/j.tecto.2016.02.022
- Somoza, L., Medialdea, T., León, R., Ercilla, G., Vázquez, J. T., Farran, M.I., et al. (2012). Structure of mud volcano systems and pockmarks in the region of the ceuta contourite depositional system (Western alborán Sea). *Mar. Geology* 332–334, 4–26. doi: 10.1016/j.margeo.2012.06.002
- Steuer, S., Franke, D., Meresse, F., Savva, D., Pubéllier, M. and Auxietre, J.-L. (2014). Oligocene–Miocene carbonates and their role for constraining the rifting and collision history of the dangerous grounds, south China Sea. *Mar. Petroleum Geology* 58, 644–657. doi: 10.1016/j.marpetgeo.2013.12.010
- Tang, W., Zhao, Z., Song, S., Wang, Y., Xie, X. and Liu, S. (2021). Differences in the tectonic evolution of basins in the central-southern south China Sea and their hydrocarbon accumulation conditions. *Acta Geologica Sin. - English Edition* 95 (1), 30–40. doi: 10.1111/1755-6724.14638
- Thran, A. C., Dutkiewicz, A., Spence, P. and Müller, R. D. (2018). Controls on the global distribution of contourite drifts: Insights from an eddy-resolving ocean model. *Earth Planetary Sci. Lett.* 489, 228–240. doi: 10.1016/j.epsl.2018.02.044
- Tian, J., Ma, X., Zhou, J. and Wang, W. (2017). Subsidence of the northern south China Sea and formation of the bashi strait in the latest Miocene: Paleooceanographic evidences from 9-myrs high resolution benthic foraminiferal  $\delta^{18}O$  and  $\delta^{13}C$  records. *Palaeogeography Palaeoclimatology Palaeoecol.* 466, 382–391. doi: 10.1016/j.palaeo.2016.11.041
- Tian, J., Wu, S., Lv, F., Wang, D., Wang, B., Zhang, X., et al. (2015). Middle Miocene mound-shaped sediment packages on the slope of the xisha carbonate platforms, south China Sea: Combined result of gravity flow and bottom current. *Deep Sea Res. Part II: Topical Stud. Oceanography* 122, 172–184. doi: 10.1016/j.dsr2.2015.06.016
- Tian, J., Yang, Q., Liang, X., Xie, L., Hu, D., Wang, F., et al. (2006). Observation of Luzon strait transport (Geophysical Research Letters 33 (19)). doi: 10.1029/2006GL026272
- Ting, K. K., Tan, Y. E., Chiew, E., Lee, E. L., Azudin, A. N. and Ishak, N. A. (2021). Assessing controls on isolated carbonate platform development in central luconia, NW Borneo, from a regional 3D seismic facies and geomorphology investigation Vol. 509 (London: Geological Society), 29. Special Publications. doi: 10.1144/SP509-2019-89
- Vahrenkamp, V. C., David, F., Duijndam, P., Newall, M. and Crevello, P. (2004). "Growth architecture, faulting, and karstification of a middle Miocene carbonate platform, luconia province, offshore Sarawak, Malaysia", in *Seismic imaging of carbonate reservoirs and systems*. Eds. Eberli, G. P., Masafiero, J. L. and Sarg, J. F. R. (American Association of Petroleum Geologists).
- Vandorpe, T. P., Van Rooij, D., Stow, D. A. V. and Henriot, J.-P. (2011). Pliocene to recent shallow-water contourite deposits on the shelf and shelf edge off south-western mallorca, Spain. *Geo-Marine Lett.* 31 (5), 391–403. doi: 10.1007/s00367-011-0248-9
- Verdicchio, G. and Trincardi, F. (2008). "Chapter 20 shallow-water contourites," in *Developments in sedimentology*. Eds. Rebesco, M. and Camerlenghi, A. (Amsterdam, NL: Elsevier), 409–433.
- Viana, A. R. (2008). "Chapter 23 economic relevance of contourites," in *Developments in sedimentology*. Eds. Rebesco, M. and Camerlenghi, A. (Amsterdam, NL: Elsevier), 491–510.
- Wagner, B., Aufgebauer, A., Vogel, H., Zanchetta, G., Sulpizio, R. and Damaschke, M. (2012). Late pleistocene and Holocene contourite drift in lake prespa (Albania/F.Y.R. @ of Macedonia/Greece). *Quaternary Int.* 274, 112–121. doi: 10.1016/j.quaint.2012.02.016
- Wang, X., Cai, F., Sun, Z., Li, Q., Li, A., Sun, Y., et al. (2022). Late Miocene–quaternary seismic stratigraphic responses to tectonic and climatic changes at the north-eastern margin of the south China Sea (Geol Soc Am Bull. ). doi: 10.1130/B36224.1
- Wang, X., Zhuo, H., Wang, Y., Mao, P., He, M., Chen, W., et al. (2018). Controls of contour currents on intra-canyon mixed sedimentary processes: Insights from the pearl river canyon, northern south China Sea. *Mar. Geology* 406, 193–213. doi: 10.1016/j.margeo.2018.09.016
- World Ocean Database. (2013). Available at: <https://www.nodc.noaa.gov/OC5/WOD13> [Accessed April 17, 2022].
- Wu, S., Zhang, X., Yang, Z., Wu, T., Gao, J. and Wang, D. (2016). Spatial and temporal evolution of Cenozoic carbonate platforms on the continental margins of the south China Sea: Response to opening of the ocean basin. *Interpretation* 4 (3), SP1–SP19. doi: 10.1190/INT-2015-0162.1
- Yang, Z., Li, X., Huang, L., Wang, L., Wu, S. and Zhang, X. (2021). Development of the Miocene guangle carbonate platform in the south China Sea: Architecture and controlling factors. *Acta Geologica Sin. - English Edition* 95 (1), 177–191. doi: 10.1111/1755-6724.14639

- Yan, Q., Shi, X., Wang, K., Bu, W. and Xiao, L. (2008). *Major element, trace element and Sr, Nd and Pb isotope studies of Cenozoic basalts from the south China Sea*. *Sci. China D Earth*. (4), 51. 550–566. doi: 10.1007/s11430-008-0026-3
- Yan, W., Zhang, G., Xia, B., Zhang, L., Yang, Z., Lei, Z., et al. (2020). Seismic characteristics and development patterns of Miocene carbonate platform in the beikang basin, southern south China Sea. *Acta Geologica Sin. - English Edition* 94 (5), 1651–1661. doi: 10.1111/1755-6724.14399
- Yan, W., Zhang, G., Zhang, L., Xia, B., Yang, Z., Lei, Z., et al. (2018). Seismic responses and distribution characteristics of the Miocene carbonate platforms in the beikang basin of southern south China Sea. *Mar. Geology Quaternary Geology* 38 (6), 118–126. doi: 10.16562/j.cnki.0256-1492.2018.06.012
- Yin, S., Hernández-Molina, F. J., Lin, L., Chen, J., Ding, W. and Li, J. (2021). Isolation of the south China Sea from the north pacific subtropical gyre since the latest Miocene due to formation of the Luzon strait. *Sci. Rep.* 11 (1), 1562. doi: 10.1038/s41598-020-79941-4
- Yin, S., Hernández-Molina, F. J., Miramontes, E., Shen, Z., Yang, C., Gao, J., et al. (2022). Sequential bedform development in mixed turbidite–contourite systems: An example from the cosmonaut Sea, East Antarctica. *Geomorphology* 410, 108287. doi: 10.1016/j.geomorph.2022.108287
- Yin, S., Hernández-Molina, F. J., Zhang, W., Li, J., Wang, L., Ding, W., et al. (2019). The influence of oceanographic processes on contourite features: A multidisciplinary study of the northern south China Sea. *Mar. Geology* 415, 105967. doi: 10.1016/j.margeo.2019.105967
- Zhang, H., Shao, L., Zhang, G., Cui, Y., Zhao, Z. and Hou, Y. (2020). The response of Cenozoic sedimentary evolution coupled with the formation of the south China Sea. *Geological J.* 55 (10), 6989–7010. doi: 10.1002/gj.3856
- Zhang, G., Tang, W., Xie, X., Zhao, Z. and Zhao, Z. (2017). Petroleum geological characteristics of two basin belts in southern continental margin in south China Sea. *Petroleum Explor. Dev.* 44 (6), 899–910. doi: 10.1016/S1876-3804(17)30102-7
- Zhou, C., Zhao, W., Tian, J., Zhao, X., Zhu, Y., Yang, Q., et al. (2017). Deep Western boundary current in the south China Sea. *Sci. Rep.* 7 (1), 9303. doi: 10.1038/s41598-017-09436-2
- Zhuo, H., Wang, Y., Shi, H., Zhu, M., He, M., Chen, W., et al. (2014). Seismic geomorphology, architecture and genesis of Miocene shelf sand ridges in the pearl river mouth basin, northern south China Sea. *Mar. Petroleum Geology* 54, 106–122. doi: 10.1016/j.marpetgeo.2014.03.002